Desalination and Water Treatment
www.deswater.com
doi: 10.5004/dwt.2021.27086

222 (2021) 271–281
May

Preparation of CQDs-TiO_2 modified activated carbon with photocatalytic regeneration properties

Jiliang Yang[a,*], Xiantian Yue[a,b], Riwu Zhang[c], Jun Ren[c]

[a]*College of Chemistry and Material Engineering, Chaohu University, Hefei 238000, China, emails: yangjiliang1984@126.com (J. Yang), yuefeiyxt@aliyun.com (X. Yue)*
[b]*College of Chemical Engineering, Nanjing Forestry University, Nanjing 210038, China*
[c]*Chaohu C-Dragon Pharmaceutical Co., Ltd., Hefei 238000, China, emails: riwuzhang@126.com (R. Zhang), renj72@163.com (J. Ren)*

Received 31 October 2020; Accepted 22 January 2021

ABSTRACT

Due to the lack of feasible regeneration methods, the waste activated carbon (AC) is often incinerated or landfilled after its adsorption applications. In this study, a self-regenerative carbon quantum dots (CQDs)-TiO_2@AC composite was built by coating CQDs-TiO_2 onto the surface of AC. Besides, the adsorption and photocatalytic regeneration performance of CQDs-TiO_2@AC was evaluated using methylene blue (MB) as a model compound. Results show that the desorption of the pollutant from the interior and surface of CQDs-TiO_2@AC played an essential role in the regeneration. The addition of H_2O_2 enhanced the generation of reactive species, such as $^{\bullet}OH$ and $^{\bullet}O_2^-$, and shortened the regeneration time. High temperature and acidic condition pushed forward the desorption of MB molecules from the sorption sites and hence promoted the regeneration. By optimizing the applied CQDs-TiO_2 dose, regeneration time, regeneration temperature, H_2O_2 dose, and pH value, ~56.39% of the adsorption capacity of the virgin CQDs-TiO_2@AC could still be retained after three cycles of MB adsorption and the photocatalytic regeneration. This study indicates that self-regenerative CQDs-TiO_2@AC composite is a type of environmentally-friendly material, and the technology is a sustainable way to regenerate spent AC for reuse.

Keywords: Methylene blue; Wastewater treatment; Adsorption; Photocatalysis; Carbon regeneration

1. Introduction

Activated carbon (AC) is the most widely-used and efficient adsorbent owing to its large surface area and high adsorption ability. However, AC cannot degrade pollutants. As a result, thrown-out saturated AC leads to severe pollution and resource waste [1]. Hence, the regeneration of spent AC has been increasingly investigated and successfully handled by many techniques, such as photo-oxidation [1], the thermal method [2], wet air oxidation [3], ultrasound [4], electrochemical regeneration [5], microwave heating [6] and bio-regeneration [7]. However, these methods usually require costly equipment investment in high pressure and temperature [8].

Photocatalytic regeneration is a promising chemical method used to purify pollutants from spent ACs. TiO_2, as one prospective photocatalyst with low cost, non-toxicity, and high chemical stability, can produce highly active photoexcited e^-/h^+ pairs under sunlight irradiation and further reacts to form high reactive radical species, such as $^{\bullet}OH$ and $^{\bullet}O_2^-$ [9]. However, the limitation of TiO_2 is the

* Corresponding author.

broad bandgap (anatase: 3.2 eV; rutile: 3.0 eV) because it solely absorbs ultraviolet (UV) light, which accounts for only 3%–5% of the solar radiation [10]. Meanwhile, the easy recombination of the photogenerated electron–hole pair in TiO_2 could reduce its photocatalytic performance. Since the competition among migration, capture, and recombination of photon-generated carrier decides the quantum efficiency and rate of photocatalytic reaction, considerable efforts have been made to enhance the quantum efficiency and photocatalytic activity by coupling with other materials, such as nonmetal elements [11], metal ions [12], and organics [13]. For example, Liu et al. [14] reported that the Ag-TiO_2 possessed higher photocatalytic ability than TiO_2; Chen et al. [15] prepared iodine-doped titanium dioxide and it exhibited better catalytic activity than titanium dioxide; Tahir et al. [16–18] prepared WO_3 composite material by compounding carbon nanofiber, active graphene and nickel ferrite and got good results. However, the additives usually are toxic, expensive and environmentally-unfriendly. Hence, it is necessary to develop materials with environmental friendliness and high photocatalytic activity for the photocatalytic regeneration process.

Carbon nanomaterials (for example, graphene, carbon nanotubes) are efficient in enhancing photocatalytic reactions because of the high electrical conductivity, huge surface area, and strong adsorption ability. Among them, carbon quantum dots (CQDs) are outstanding with chemical stability, broad absorption spectrum, high absorption ability, and high photoelectron transfer ability [19]. CQDs composited with TiO_2 (CQDs-TiO_2) are widely used to degrade azo dyes and methylene blue (MB) and to catalyze hydrogen evolution reactions [20,21]. As reported, the photocatalytic efficiency of CQDs/TiO_2 composite is higher than that of pristine TiO_2 nanofibers [22]. Thus, it is anticipated that CQDs/TiO_2 composite would have high regeneration efficiency in photocatalysis. Besides, CQDs/TiO_2 composite is more environmentally friendly because of the low toxicity of CQDs. Based on the above assumptions, we propose a new regenerable composite by impregnating AC with CQDs/TiO_2 to achieve AC *in situ* regeneration by photocatalysis.

This study aims to prepare a photocatalytic self-regenerative CQDs-TiO_2@AC composite with high adsorption and regeneration performances for environmental purification. The combination was achieved by coating the CQDs-TiO_2 onto the surface of AC as a modifying agent. MB was chosen as a target pollutant since it is the most common water–soluble cationic dye with toxicity and high chromaticity in industrial pollutant headstreams [23–26]. MB removal experiments evaluated the photocatalytic adsorption and degradation performance of CQDs-TiO_2@AC. Besides, the regeneration efficiency of this composite saturated with MB during photocatalysis was evaluated. Furthermore, the impacts of temperature, pH, and photocatalysis time on photocatalytic regeneration were studied.

2. Materials and methods

2.1. Materials

A commercial coconut-shell-based AC was used in this investigation (40 mesh; Tianjin Guang Fu Technology Development Co., Ltd., China). Before use, AC was added in 300 mL of a 0.1 mol L^{-1} HNO_3 solution under stirring at 40°C for 2 h. The mixture was then filtered, washed with boiling water until the filtrate reached pH = 7, and then dried at 105°C overnight. All other chemicals were purchased from Xilong Reagent Company (Guangdong Province, China) and used as received. Deionized water was used throughout.

2.2. Synthesis of CQDs, CQDs-TiO_2, and CQDs-TiO_2@AC

CQDs were synthesized in our previous work [27]. Firstly, 0.7 g of tris(hydroxymethyl)aminomethane was added to 30 mL of H_2O containing citric acid (1.0 g). The resulting mixture was removed into a 100 mL Teflon lined stainless steel autoclave, which was ultrasonically treated for 30 min and then oven-heated constantly at 170°C for 4.5 h. Finally, the solution containing CQDs was dialyzed against deionized water in a dialysis bag (3,500 Da) for 12 h and freeze-dried.

CQDs-TiO_2 was prepared as follows [28] with minor modifications: 5 g of a tetra-n-butyl titanate was mixed with 10 mL of 100 mg L^{-1} CQDs solution under stirring at room temperature to form a homogeneous mixed solution. The mixed solution was then put into a new autoclave, which was continuously heated at 160°C for 12 h. The products were washed with water and ethanol several times and vacuum-dried at 80°C. TiO_2 was synthesized by the same method without the addition of CQDs.

The self-regenerative composite CQDs-TiO_2@AC was synthesized as follows: 5 g of AC and x wt.% (x = 1, 3, 5, 7) of CQDs-TiO_2 were dispersed into water under continuous stirring for 1 h. Subsequently, the mixture was filtered and dried at 85°C for 12 h.

2.3. Photocatalytic degradation experiment

The photocatalytic degradation efficiency of MB was tested as follows: a sample (1.0 g) was added into 1,000 mL of an MB solution (20 mg L^{-1}) under stirring and UV irradiation (2 × 30 W, λ = 254 nm, JT8-Y30W, Weiersi, China). During the experiment, aliquots of the suspension were sampled at a certain time interval and centrifuged (3,000 rpm, 5 min) to remove the catalyst particles. Then the supernatant liquid concentration was determined by UV-Vis spectroscopy (λ_{max} = 665 nm). The photocatalytic degradation efficiency η was calculated as follows [15]:

$$\eta = \frac{\left(C_0 - C_t\right)}{C_0} \times 100\% \quad (1)$$

where C_0 and C_t (mg L^{-1}) are the MB concentrations initially and at time t, respectively.

2.4. Regeneration experiment

The exhausted CQDs-TiO_2@AC (3 wt.% CQDs-TiO_2) was prepared by soaking CQDs-TiO_2@AC in a 1 g L^{-1} MB solution at a CQDs-TiO_2@AC to solution ratio of 1 g L^{-1} for 24 h in the dark. Subsequently, the suspension was filtered, and CQDs-TiO_2@AC saturated with MB was dried at 85°C for 6 h.

The photocatalytic regeneration of exhausted CQDs-TiO_2@AC was carried out in a 1 L transparent glass photoreactor. The MB-saturated CQDs-TiO_2@AC (1.0 g) was added into 800 mL of water, and a 30 W spiral UV lamp (λ = 365 nm, JND-1027, Donglang, China) was directly inserted into the water to the depth of about 6 cm. At the same time, the suspension was air-bubbled at a flow rate of 50 mL min^{-1}. After the regeneration experiment, CQDs-TiO_2@AC was filtered and dried at 95°C for 12 h. Furthermore, the regeneration efficiency of CQDs-TiO_2@AC was evaluated by comparing the MB adsorption capacity between the regenerated carbon and the fresh carbon under the same conditions. The adsorption capacity q_e (mg g^{-1}) was calculated as follows [15]:

$$q_e = \frac{\left(C_0 - C_t\right)V}{m} \tag{2}$$

where V (L) is the MB solution volume; m (g) is the mass of CQDs-TiO_2@AC.

The regeneration efficiency RE (%) of CQDs-TiO_2@AC was calculated as follows [15]:

$$\mathrm{RE} = \frac{q_{e,r}}{q_{e,f}} \times 100\% \tag{3}$$

where $q_{e,r}$ and $q_{e,f}$ (mg g^{-1}) are the adsorption capacity of regenerated and fresh CQDs-TiO_2@AC containing 3 wt.% CQDs-TiO_2, respectively.

2.5. Characterization

Morphology of CQDs was tested by an FEI Tecnai G2 F20 transmission electron microscope (TEM). The surface morphology of CQDs-TiO_2 and CQDs-TiO_2@AC was observed under a Hitachi S-4800 (Japan) scanning electron microscope (SEM). Crystallography of all samples was recorded by an X-ray diffractometer (XRD, D/MAX 2500PC, Rigaku Co., Japan) under Cu Kα radiation from 2θ = 5° to 80°. X-ray photoelectron spectroscopy (XPS) was obtained using a Kratos Axis Ultra HAS-Vision X-ray photoelectron spectrometer with a monochromatized Al Kα radiation (Kratos Analytical Ltd., UK). Fourier transform infrared (FTIR) spectra from 4,000 to 400 cm^{-1} were detected on an FTIR-650 spectrometer (Tianjin Gangdong Sci. & Tech. Development Co., Ltd., China). UV-Vis spectroscopy was carried out with a UV-5100B spectrometer (Shanghai Metash Instruments Co., Ltd., China).

3. Results and discussion

3.1. Characterization

Fig. 1 shows the morphology characterized by TEM and SEM. CQDs are nearly spherical nanoparticles in a diameter of around 5~15 nm (Fig. 1a). CQDs-TiO_2 (Fig. 1b) shows that the composite particles are mostly around ball shape and agglomerated together. Additionally, different CQDs-TiO_2 particles appear on the porous surface of AC (Fig. 1c). A high-resolution transmission electron microscope (HRTEM) was also further used to reveal the elaborate structure of composite CQDs-TiO_2 (Fig. 1d). The lattice spacing of about 0.35 nm in the HRTEM image is consistent with the (101) plane of anatase titanium dioxide. The spherical particle with a diameter of about 10 nm marked with a white circle corresponds to CQDs, indicating that CQDs were combined with TiO_2 and formed CQDs-TiO_2 composite. In summary, the conclusions show that the CQDs-TiO_2 was successfully absorbed on the surface and in the micropores of AC through the dipping process. Since the pores of AC play an essential role in adsorption, the adsorption performance of CQDs-TiO_2@AC will differ among different loads of CQDs-TiO_2 due to different extents of pore blockages. In conclusion, loaded-CQDs-TiO_2 affects the adsorption property of AC, and it was further confirmed by textural characterization.

Table 1 indicates the textural parameters. According to Table 1, the Brunauer–Emmett–Teller (BET) surface areas and micropore volumes are affected by CQDs-TiO_2 loading on AC. The textural properties are reduced as the amount of CQDs-TiO_2 increases. The nitrogen adsorption and desorption isotherms of samples as shown in Fig. S1 indicate similar results.

Fig. 2 shows the XRD patterns of the samples. The diffraction peaks at 2θ = 54.38°, 62.72°, 69.04° and 70.06° in the curves of both TiO_2 and CQDs-TiO_2 correspond to the (211), (002), (301) and (112) planes, respectively, indicating both TiO_2 and CQDs-TiO_2 well agree with rutile phases. The peaks at 2θ = 25.28°, 37.86°, and 47.89° represent the (101), (004) and (105) planes, respectively and reveal the formation of anatase TiO_2. In comparison, the peak at 2θ = 25° on the curve of CQDs-TiO_2@AC right-shifts, and five new weak peaks appear at 2θ = 37.86°, 47.89°, 54.38°, 62.72° and 75.50°, which suggest the presence of CQDs-TiO_2 on the surface of AC. Furthermore, CQDs-TiO_2 was impregnated under regeneration conditions and then tested by XRD to confirm the stability during the operation. As shown in Fig. S2, the XRD testing results are similar, indicating that the structure of CQDs-TiO_2 has not changed. We tested 3% CQDs-TiO_2@AC in the same way and got similar results (Fig. S3).

FTIR spectra of samples are illustrated in Fig. 3. The peaks around 3,440; 1,715; 1,630; 1,243; 1,100 and 520 cm^{-1} are associated with the stretching vibrations of O–H, C=O, C=C, C–O, O–H, and Ti–O, respectively. Moreover, the peak of CQDs-TiO_2 below 1,000 cm^{-1} is broader and blue-shifts compared with TiO_2, which may be due to the combined vibration of Ti–O–Ti and Ti–O–C and suggests the CQDs and TiO_2 were coupled by the formation of Ti–O–C [29].

XPS spectra were further explored to characterize the synthesized 5% CQDs-TiO_2@AC. Fig. 4 are the XPS full spectrum diagrams of the sample, and the peak analytical spectrum diagrams of C1s, O1s and Ti_{2p}, respectively. Fig. 4a shows peaks of C_{1s}, N_{1s}, O_{1s} and Ti_{2p}, indicating that the surface of the sample has C (89.48%), N (1.65%), O (4.12%) and Ti (4.75%) elements. The high-resolution C1s XPS spectrum (Fig. 4b) exhibited three peaks at 284.4, 285.7, and 288.7 eV, associated with C=C, C–O and C=O bonds, respectively. As shown in Fig. 4c, the peak centered at 530.8 eV is due to Ti–O function group in TiO_2, while the peaks at 532.4 and 533.6 eV are associated with C=O and C–O bonds on the CQDs surface, respectively. Then it can be inferred that the sample particles contain CQDs and TiO_2. Fig. 4c illustrates

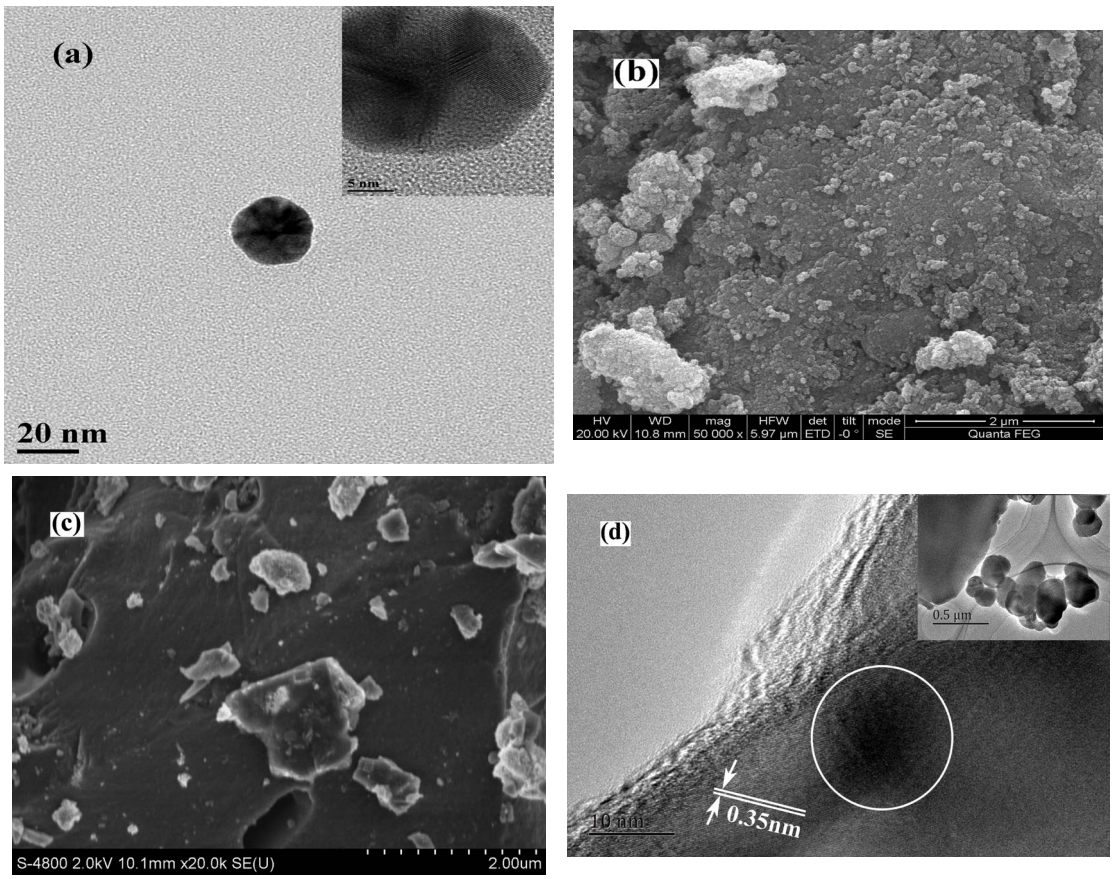

Fig. 1. (a) HRTEM image of CQDs; (b) SEM image of CQDs-TiO_2, (c) CQDs-TiO_2@AC and (d) HRTEM of CQDs-TiO_2.

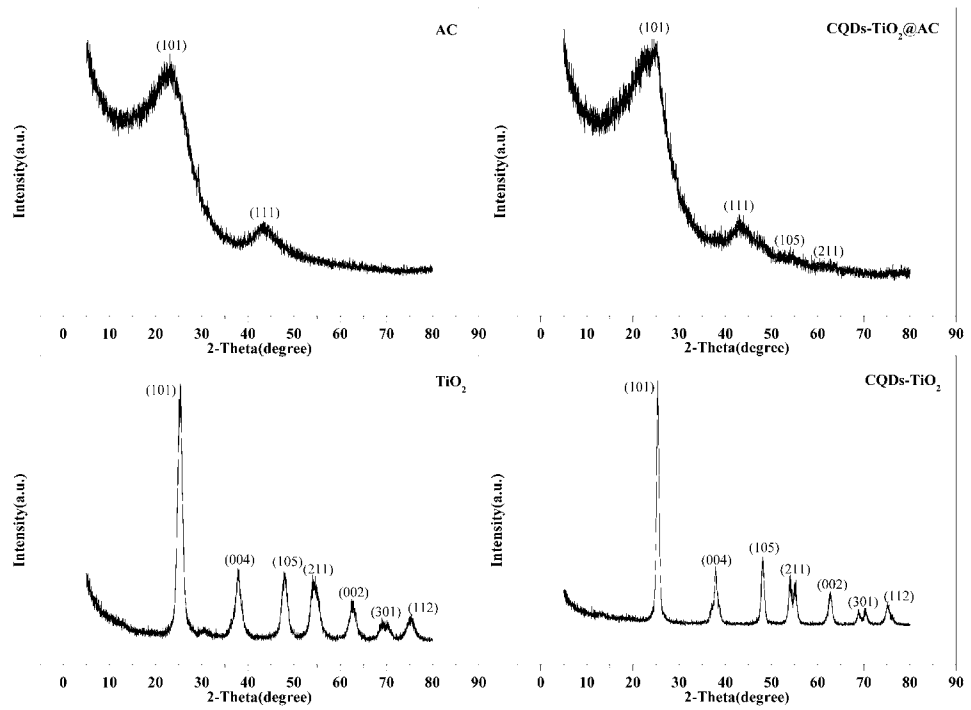

Fig. 2. XRD patterns of samples.

Table 1
Textural characterization of samples

Characterization	AC	1%CQDs-TiO_2@AC	3%CQDs-TiO_2@AC	5%CQDs-TiO_2@AC
BET surface area ($m^2\ g^{-1}$)	621	551	471	388
Micropore volume ($cm^3\ g^{-1}$)	0.2573	0.2209	0.2034	0.1883

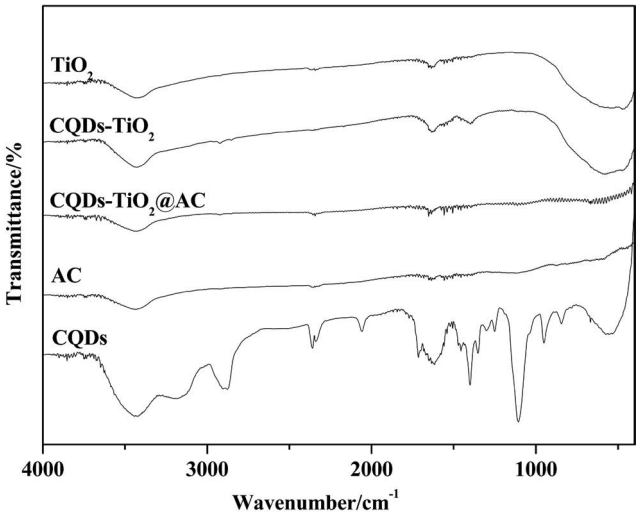

Fig. 3. FTIR spectra of samples.

the high-resolution XPS spectrum diagram of Ti_{2p}, which exhibits peaks at around 459.7 and 465.5 eV, corresponding to TiO_2 electron binding energies $Ti2p_{3/2}$ and $Ti2p_{1/2}$, respectively [30]. The above observation is consistent with the XRD result, showing that the TiO_2 in the sample particles is anatase-type TiO_2.

3.2. Photocatalytic degradation of MB

The results of MB degradation efficiency under UV irradiation are shown in Fig. 5 and Table 2. The MB degradation efficiency rates of TiO_2 and CQDs-TiO_2 at 120 min are 58.9% and 78.2%, respectively (Fig. 5a), indicating that the introduction of CQDs could considerably strengthen the photocatalytic ability of TiO_2. During the MB removal by CQDs-TiO_2@AC, MB molecules firstly immigrated from the aqueous solution to the surface of AC, indicating that AC played a crucial role in gathering. Then photocatalytic degradation occurred [31]. As for CQDs-TiO_2@AC integrating the advantages of AC and CQDs-TiO_2, the MB removal resulted from the synergy between adsorption and photocatalytic degradation. Additionally, CQDs acting as an electron acceptor could decelerate electron-hole recombination and enhance photocatalytic efficiency.

Furthermore, the MB degradation efficiency of CQDs-TiO_2@AC was affected by the load of CQDs-TiO_2. In one respect, the amounts of reactive species such as $^{\bullet}OH$ and $^{\bullet}O_2^-$ generated by CQDs-TiO_2 under UV irradiation rose with the increasing load, which enhanced the contact probability with MB molecules and then promoted the pollutant degradation [32]. However, with the higher load of CQDs-TiO_2, the micropores significantly blocked the surface of AC and further impacted the adsorption properties of AC. The adsorption rates were decelerated with the increasing load of CQDs-TiO_2 because there are fewer active sites for the adsorption of adsorbent molecules when the load was higher than 3 wt.%. Then the photocatalytic activity decreased together with degradation efficiency.

The MB decay during photocatalytic degradation under UV irradiation was fitted with a pseudo-first-order equation: $-\ln(C_t/C_0) = kt$, where k is the photocatalytic reaction rate constant and t is irradiation time. The values of k for TiO_2 and CQDs-TiO_2 were 0.0063, and 0.0123 min^{-1}, respectively (Fig. 5b), which proved the photocatalytic activity of CQDs-TiO_2 was higher than TiO_2. Noticeably, k rose with the increasing load of CQDs-TiO_2 when the load was below 3 wt.%, but decreased when the load was 5–7 wt.%. This phenomenon may be attributed to that the amount of CQDs-TiO_2 occupying the specific surface area and total pore volume of the AC increased, leading to a decrease in the adsorption capacity of AC [33]. It corresponds to the textural characterization as shown in Table 1. Furthermore, the blocked pores negatively influence the oxidation reaction, so that the regeneration efficiency of CQDs-TiO_2@AC composite decreases [34]. Moreover, k maximized at the load of 3 wt.%, suggesting 3% CQDs-TiO_2@AC was the optimum photocatalyst and thus was used as a self-regenerative photocatalyst in the subsequent regeneration experiments.

In summary, CQDs-TiO_2@AC obtains better photocatalytic activity in three ways: (1) the accelerated aggregation of pollutant molecules on the surface of the photocatalyst, (2) the improved contact probability between reactive species and pollutant molecules, and (3) the slower recombination of electron–hole pair.

3.3. Regeneration experiments

MB removal by CQDs-TiO_2@AC was characterized as adsorption-photocatalytic bifunction. In contrast, the regeneration of spent AC consisted of two stages: the pollutant (1) was decomposed by reactive species and migrated from pore channels to the surface of CQDs-TiO_2@AC, and (2) was degraded by photocatalysis. Furthermore, the desorption rate is the core influence factor on regeneration efficiency in the first stage. Therefore, influencing factors such as regeneration time, regeneration temperature, H_2O_2, and pH were investigated.

3.3.1. Effect of regeneration time

The effect of regeneration time on the regeneration of exhaust CQDs-TiO_2@AC is depicted in Fig. 6a and Table S1. The regeneration efficiency almost stabilizes around 45% at

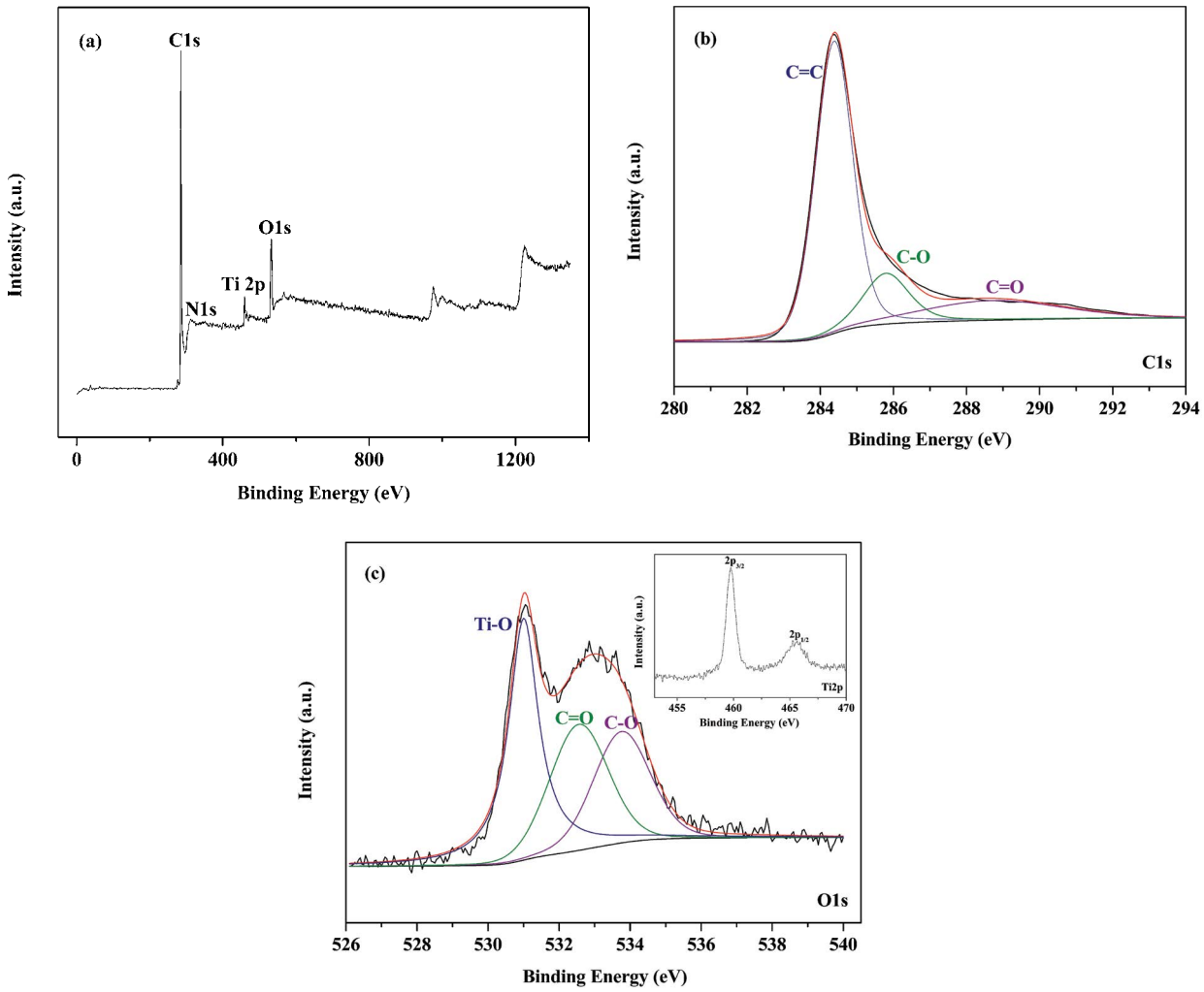

Fig. 4. XPS spectrum of 5% CQDs-TiO_2@AC.

Table 2
Degradation efficiency of samples on MB

Sample		UV irradiation time/min					
		20	40	60	80	100	120
AC	C_e (mg L^{-1})	8.09	4.76	3.68	1.31	0.79	0.48
	Degradation (%)	59.57	76.22	81.61	93.46	96.06	97.59
TiO_2	C_e (mg L^{-1})	16.47	14.60	12.42	10.99	9.55	8.22
	Degradation (%)	17.63	27.02	37.89	45.04	52.24	58.92
CQDs-TiO_2	C_e (mg L^{-1})	14.28	11.12	9.90	7.77	5.30	4.36
	Degradation (%)	28.62	44.40	50.51	61.14	73.52	78.20
1%CQDs-TiO_2@AC	C_e (mg L^{-1})	8.33	5.86	3.84	2.83	1.47	0.67
	Degradation (%)	58.33	70.70	80.81	85.85	92.63	96.65
3%CQDs-TiO_2@AC	C_e (mg L^{-1})	5.66	2.38	1.50	0.74	0.42	0.26
	Degradation (%)	71.70	88.11	92.50	96.30	97.92	98.70
5%CQDs-TiO_2@AC	C_e (mg L^{-1})	10.55	8.79	7.70	5.60	3.36	1.53
	Degradation (%)	47.26	56.06	61.51	72.03	83.21	92.33
7%CQDs-TiO_2@AC	C_e (mg L^{-1})	12.99	10.90	9.90	8.38	8.12	6.18
	Degradation (%)	35.06	45.54	50.48	58.12	59.39	69.09

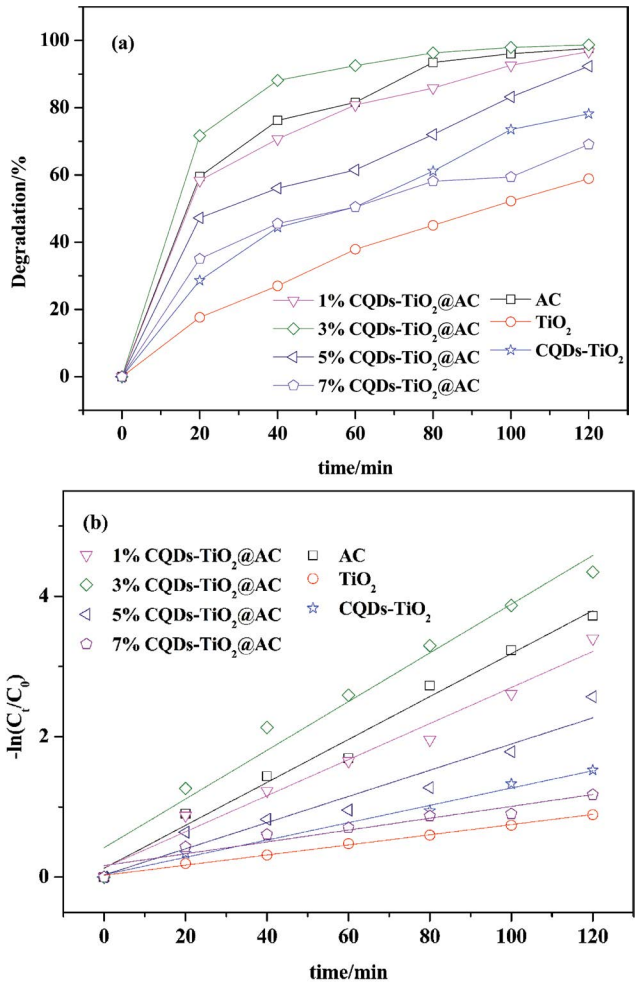

Fig. 5. (a) Degradation efficiency of samples on MB and (b) $-\ln(C_t/C_0)$ vs. t plots for the MB photodegradation by samples.

about 20 h (Fig. 6a). The regeneration efficiency is gradually enhanced with a prolonged regeneration time. Besides, the curve of regeneration efficiency is steep at the regeneration time less than 8 h and then changes gently, which may be related to the desorption rate of MB molecules. In brief, the MB molecules adsorbed on the surface of CQDs-TiO_2@AC can be desorbed quickly and degraded firstly. At the same time, the intermediates deposit on the surface and pores, resulting in the failed migration of pollutant molecules in deep pore channels and a small change of regeneration efficiency. Similarly, Chiu et al. [35] revealed that the pollutant molecules were easily adsorbed by AC and oxidized by hydroxyl radicals. In addition, the limited regeneration was also attributed to the irreversible and limited pollutant molecules that were desorbed in AC [36]. Therefore, MB-saturated ACs cannot be effectively regenerated by simple desorption-based techniques [37].

3.3.2. Effect of H_2O_2

H_2O_2 can enhance photocatalysis since it acts as an electron acceptor to preferentially react with TiO_2 to produce numerous reactive species, such as •OH [8]. Thus, the addition of H_2O_2 favors the reaction between •OH and adsorbed contaminants and promotes oxidation efficiency [36]. The effect of H_2O_2 was also explored (Fig. 6b and Table S2). With the addition of 1.5 mmol L^{-1} H_2O_2 into the regeneration system, the regeneration efficiency was balanced faster compared with that without H_2O_2, but the final regeneration efficiency was not influenced. The results are consistent with a report [14].

Table 3
Regeneration efficiencies and adsorption capacities obtained during the 3 consecutive photocatalytic regeneration cycles of MB-saturated CQDs-TiO_2@AC under optimized conditions

	Cycle of photocatalytic regeneration			
	0	1	2	3
q_e (mg g^{-1})	5.99	3.99	3.75	3.38
Regeneration efficiency (%)	–	66.62	62.60	56.39

3.3.3. Effect of regeneration temperature

It is generally believed that high temperature is beneficial for the mass transfer of pollutants in desorption. Fig. 6c and Table S3 show the effects of regeneration temperature on regeneration efficiency. The regeneration efficiency was improved with the temperature rise, suggesting that higher temperatures contributed to the regeneration of CQDs-TiO_2@AC composite. The reason may be that the higher temperature was beneficial for MB molecules' desorption and could fasten the reagent pervasion rate into the micropores [27,14].

3.3.4. Effect of pH

The pH influences not only the surface charge of carbon but also the ionization state of dissolved materials in AC/solution mixture [34]. At both positive and negative zeta potentials of the surface of the composite, the accumulation of the cation MB is dominated by electrostatic attraction. Since high pH will enhance the surface negative properties and the MB adsorption and photocatalytic degradation, the conditions do not benefit the desorption of MB during regeneration. Along with the variation of pH, the regeneration efficiency increases under acidic conditions (Fig. 6d and Table S4). Under the conditions of CQDs-TiO_2 loading of 3 wt.%, the regeneration time of 20 h, H_2O_2 addition of 1.5 mmol L^{-1}, regeneration temperature at 65°C and pH 6, the regeneration efficiency is about 60.7%.

3.3.5. Effect of adsorption and regeneration cycles

To evaluate the reusability of the CQDs-TiO_2@AC, 3 circles of MB adsorption and photocatalytic regeneration were explored. Fig. 7 and Table 3 show that the regeneration efficiencies decreased gradually over the 3 cycles of adsorption and regenerations. There is ~56% of the adsorption capacity of the virgin CQDs-TiO_2@AC could still be retained after 3 cycles of the photocatalytic regeneration. Furthermore, the textural properties of CQDs-TiO_2@AC after

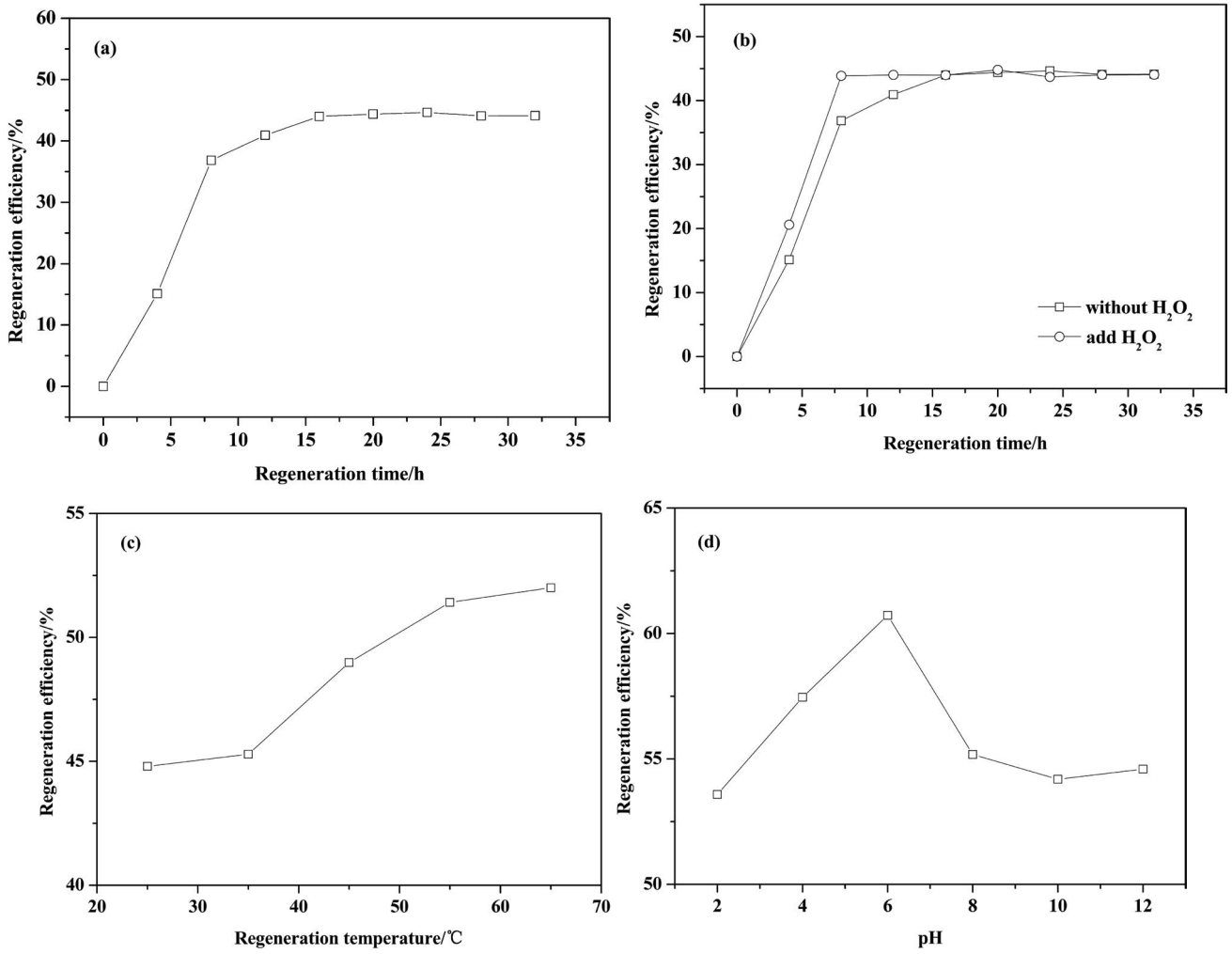

Fig. 6. Effects of (a) regeneration time, (b) H_2O_2, (c) regeneration temperature (H_2O_2 addition of 1.5 mmol L^{-1}; regeneration time = 20 h) and (d) pH (H_2O_2 addition of 1.5 mmol L^{-1}; regeneration time = 20 h; regeneration temperature = 65°C).

3 cycles of the photocatalytic regeneration were characterized by BET analysis (Table S5). The results show that the BET surface area and micropore volume of the sample are reduced to 231 $m^2 g^{-1}$ and 0.1145 $cm^3 g^{-1}$, respectively. It may be because of the accumulation of incompletely degraded MB and degradation products on the surface of the sample which causes pore blockage.

4. Conclusions

This work introduced the photocatalytic process as a promising alternative for the *in situ* regeneration of wasted CQDs-TiO_2@AC. By oxidizing the sorbed MB through reactive species (such as $^{\bullet}OH$ and $^{\bullet}O_2^-$) to oxidation by-products, the photocatalytic regeneration could restore (>60%) the adsorption capacity of MB-saturated CQDs-TiO_2@AC. Furthermore, the addition of H_2O_2 helped to generate more reactive species and accelerated regeneration. High temperature and acidic conditions were beneficial for the desorption of MB molecules from the interior and the surface of CQDs-TiO_2@AC. During the photocatalytic regeneration, the oxidation by-products and incompletely degraded MB were accumulated on the surface of the composite, leading to a gradual decrease in the microporosity and thus reducing the adsorption capacity for subsequent adsorption cycles. By optimizing the applied CQDs-TiO_2 dose, regeneration time, regeneration temperature, H_2O_2 dose, and pH value, ~56.39% of the adsorption capacity of the virgin CQDs-TiO_2@AC could still be retained after three cycles of MB adsorption and the photocatalytic regeneration. This photocatalytic regeneration process has the advantages of reduced investment in equipment and simplified operation, making the CQDs-TiO_2@AC composite an environmentally-friendly material to reduce environmental stress.

Acknowledgments

This research was supported by the Dr. Start-up Foundation of Chaohu University (KYQD-201602), School-level Scientific Research Projects of Chaohu University (XLY-201607, XLZ-201805, XLZ-201806), and Natural Science

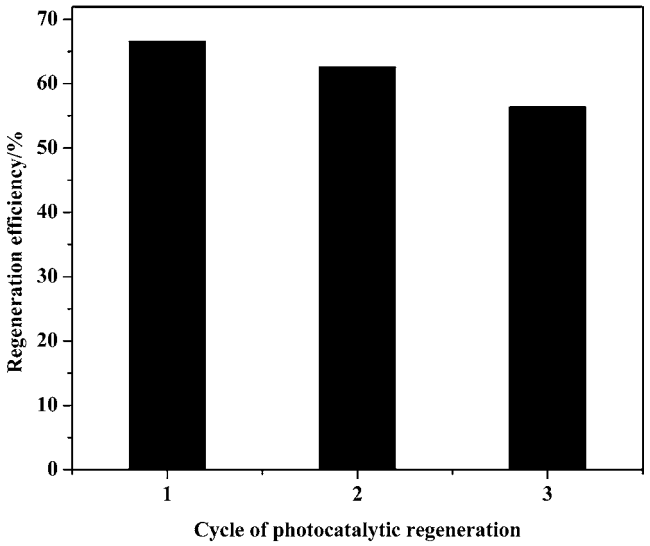

Fig. 7. Regeneration efficiencies obtained during the 3 consecutive photocatalytic regeneration cycles of MB-saturated CQDs-TiO_2@AC under optimized conditions.

Research Project in Colleges and Universities of Anhui Province (KJ2019A0678).

Symbols

η	—	Photocatalytic degradation efficiency, %
C_0	—	Initially concentrations of MB, mg L^{-1}
C_t	—	Concentrations of MB at time t, mg L^{-1}
q_e	—	Adsorption capacity, mg g^{-1}
RE	—	Regeneration efficiency, %
$q_{e,r}$	—	Adsorption capacity of regenerated CQDs-TiO_2@AC containing 3 wt.% CQDs-TiO_2, mg g^{-1}
$q_{e,f}$	—	Adsorption capacity of fresh CQDs-TiO_2@AC containing 3 wt.% CQDs-TiO_2, mg g^{-1}
k	—	Photocatalytic reaction rate constant
t	—	Irradiation time, min

Abbreviations

AC	—	Activated carbon
CQDs	—	Carbon quantum dots
MB	—	Methylene blue
UV	—	Ultraviolet
TEM	—	Transmission electron microscope
SEM	—	Scanning electron microscope
XRD	—	X-ray diffractometer
FTIR	—	Fourier transform infrared

References

[1] S.K. Al-Dawery, Adsorption of methanol from methanol–water mixture by activated carbon and its regeneration using photo-oxidation process, Desal. Water Treat., 57 (2016) 3065–3073.
[2] B. Ledesma, S. Román, A. Álvarez-Murillo, E. Sabio, J.F. González, Cyclic adsorption/thermal regeneration of activated carbons, J. Anal. Appl. Pyrolysis, 106 (2014) 112–117.
[3] C.L. Mangun, K.R. Benak, M.A. Daley, J. Economy, Oxidation of activated carbon fibers: effect on pore size, surface chemistry, and adsorption properties, Chem. Mater., 11 (1999) 3476–3483.
[4] S. Guilane, O. Hamdaoui, Ultrasound-assisted regeneration of granular activated carbon saturated by 4-chlorophenol in batch-loop reactor, Desal. Water Treat., 57 (2016) 17262–17270.
[5] R.V. Mcquillan, G.W. Stevens, K.A. Mumford, The electrochemical regeneration of granular activated carbons: a review, J. Hazard. Mater., 355 (2018) 34–49.
[6] R. Cherbański, Regeneration of granular activated carbon loaded with toluene – comparison of microwave and conductive heating at the same active powers, Chem. Eng. Process., 123 (2018) 148–157.
[7] M. El Gamal, H.A. Mousa, M.H. El-Naas, R. Zacharia, S.J. Judd, Bio-regeneration of activated carbon: a comprehensive review, Sep. Purif. Technol., 197 (2018) 345–359.
[8] R.S. Horng, I.-C. Tseng, Regeneration of granular activated carbon saturated with acetone and isopropyl alcohol via a recirculation process under H_2O_2/UV oxidation, J. Hazard. Mater., 154 (2008) 366–372.
[9] K. Guan, Relationship between photocatalytic activity, hydrophilicity and self-cleaning effect of TiO_2/SiO_2 films, Surf. Coat. Technol., 191 (2005) 155–160.
[10] J. Chen, J. Shu, A. Zhang, J.Y. Heng, Z.Y. Yan, J.Q. Chen, Synthesis of carbon quantum dots/TiO_2 nanocomposite for photo-degradation of Rhodamine B and cefradine, Diamond Relat. Mater., 70 (2016) 137–144.
[11] K.F. Zhou, Y.H. Zhu, X.L. Yang, X. Jiang, C.Z. Li, Preparation of graphene–TiO_2 composites with enhanced photocatalytic activity, New J. Chem., 35 (2011) 353–359.
[12] S.A.K. Leghari, S. Sajjad, F. Chen, J.L. Zhang, WO_3/TiO_2 composite with morphology change via hydrothermal template-free route as an efficient visible light photocatalyst, Chem. Eng. J., 166 (2011) 906–915.
[13] B.A. van Driel, P.J. Kooyman, K.J. van den Berg, A. Schmidt-Ott, J. Dik, A quick assessment of the photocatalytic activity of TiO_2 pigments — from lab to conservation studio!, Microchem. J., 126 (2016) 162–171.
[14] S.X. Liu, C. Sun, S.R. Zhang, Photocatalytic regeneration of exhausted activated carbon saturated with phenol, Bull. Environ. Contam. Toxicol., 73 (2004) 1017–1024.
[15] J. Chen, Y.F. Qin, Z.H. Chen, Z. Yang, W.B. Yang, Y.P. Wang, Gas circulating fluidized beds photocatalytic regeneration of I-TiO_2 modified activated carbons saturated with toluene, Chem. Eng. J., 293 (2016) 281–290.
[16] M.B. Tahir, A.M. Asiri, G. Nab, M. Rafique, M. Sagir, Fabrication of heterogeneous photocatalysts for insight role of carbon nanofibre in hierarchical WO_3/$MoSe_2$ composite for enhanced photocatalytic hydrogen generation, Ceram. Int., 45 (2019) 5547–5552.
[17] M.B. Tahir, G. Nabi, N.R. Khalid, Enhanced photocatalytic performance of visible-light active graphene-WO_3 nanostructures for hydrogen production, Mater. Sci. Semicond. Process., 84 (2018) 36–41.
[18] M.B. Tahir, Microbial photoelectrochemical cell for improved hydrogen evolution using nickel ferrite incorporated WO_3 under visible light irradiation, Int. J. Hydrogen Energy, 44 (2019) 17316–17322.
[19] S.Y. Lim, W. Shen, Z.Q. Gao, Carbon quantum dots and their applications, Chem. Soc. Rev., 44 (2015) 362–381.
[20] J. Tian, Y.H. Leng, Z.H. Zhao, Y. Xia, Y.H. Sang, P. Hao, J. Zhan, M.C. Li, H. Liu, Carbon quantum dots/hydrogenated TiO_2 nanobelt heterostructures and their broad spectrum photocatalytic properties under UV, visible, and near-infrared irradiation, Nano Energy, 11 (2015) 419–427.
[21] Q. Chang, K.K. Li, S.L. Hu, Y.G. Dong, J.L. Yang, Hydroxyapatite supported N-doped carbon quantum dots for visible-light photocatalysis, Mater. Lett., 175 (2016) 44–47.
[22] P.S. Saud, B. Pant, A.-M. Alam, Z.K. Ghouri, M. Park, H.-Y. Kim, Carbon quantum dots anchored TiO_2 nanofibers: effective photocatalyst for waste water treatment, Ceram. Int., 41 (2015) 11953–11959.

[23] A.A. Narvekar, J.B. Fernandes, S.G. Tilve, Adsorption behavior of methylene blue on glycerol based carbon materials, J. Environ. Chem. Eng., 6 (2018) 1714–1725.
[24] J.T. Adeleke, T. Theivasanthi, M. Thiruppathi, M. Swaminathan, T. Akomolafe, A.B. Alabi, Photocatalytic degradation of methylene blue by ZnO/$NiFe_2O_4$ nanoparticles, Appl. Surf. Sci., 455 (2018) 195–200.
[25] A.S. Ibupoto, U.A. Qureshi, F. Ahmed, Z. Khatri, M. Khatri, M. Maqsood, R.Z. Brohi, I.S. Kim, Reusable carbon nanofibers for efficient removal of methylene blue from aqueous solution, Chem. Eng. Res. Des., 136 (2018) 744–752.
[26] D. Pathania, S. Sharma, P. Singh, Removal of methylene blue by adsorption onto activated carbon developed from *Ficus carica* bast, Arabian J. Chem., 10 (2017) S1445–S1451.
[27] J.L. Yang, L. Chen, Q.Q. Jiang, X.T. Yue, Optimized preparation of nitrogen-doped carbon dots by response surface methodology and application in Cd^{2+} detection, Fullerenes Nanotubes Carbon Nanostruct., 27 (2019) 233–239.
[28] Y.-Q. Zhang, D.-K. Ma, Y.-G. Zhang, W. Chen, S.-M. Huang, N-doped carbon quantum dots for TiO_2-based photocatalysts and dye-sensitized solar cells, Nano Energy, 2 (2013) 545–552.
[29] N.C.T. Martins, J. Ângelo, A.V. Girao, T. Trindade, L. Andrade, A. Mendes, N-doped carbon quantum dots/TiO_2 composite with improved photocatalytic activity, Appl. Catal., B, 193 (2016) 67–74.
[30] B. Zhang, H. Maimaiti, D.-D. Zhang, B. Xu, M. Wei, Preparation of coal-based C-dots/TiO_2 and its visible-light photocatalytic characteristics for degradation of pulping black liquor, J. Photochem. Photobiol., A, 345 (2017) 54–62.
[31] T.S. Natarajan, H.C. Bajaj, R.J. Tayade, Palmyra tuber peel derived activated carbon and anatase TiO_2 nanotube based nanocomposites with enhanced photocatalytic performance in rhodamine 6G dye degradation, Process Saf. Environ. Prot., 104 (2016) 346–357.
[32] S. Natarajan, H.C. Bajaj, R.J. Tayade, Recent advances based on the synergetic effect of adsorption for removal of dyes from waste water using photocatalytic process, J. Environ. Sci., 30 (2018) 201–222.
[33] Z.H. Hu, T. Xu, B.W. Fang, Photocatalytic degradation of vehicle exhaust using Fe-doped TiO_2 loaded on activated carbon, Appl. Surf. Sci., 420 (2017) 34–42.
[34] Q.M. Li, Y.S. Qi, C.Z. Gao. Chemical regeneration of spent powdered activated carbon used in decolorization of sodium salicylate for the pharmaceutical industry, J. Cleaner Prod., 86 (2015) 424–431.
[35] C.-A. Chiu, K. Hristovski, S.G. Huling, P. Westerhoff, In-situ regeneration of saturated granular activated carbon by an iron oxide nanocatalyst, Water Res., 47 (2013) 1596–1603.
[36] R.M. Narbaitz, J. McEwen, Electrochemical regeneration of field spent GAC from two water treatment plants, Water Res., 46 (2012) 4852–4860.
[37] S.T. Liu, Y.J. Wang, B. Wang, J. Huang, S.B. Deng, G. Yu, Regeneration of Rhodamine B saturated activated carbon by an electro-peroxone process, J. Cleaner Prod., 168 (2017) 584–594.

Supporting information

Table S1
Effect of regeneration time

Sample	Regeneration time (h)								
	0	4	8	12	16	20	24	28	32
$q_{e,r}$ (mg g^{-1})	–	1.64	4.00	4.44	4.77	4.81	4.84	4.78	4.79
RE (%)	0	15.11	36.85	40.93	44.00	44.38	44.65	44.10	44.14

Table S2
Effect of H_2O_2

Sample		Regeneration time (h)								
		0	4	8	12	16	20	24	28	32
Without H_2O_2	$q_{e,r}$ (mg $g^{-1)}$	–	1.64	4.00	4.44	4.77	4.81	4.84	4.78	4.79
	RE (%)	0	15.11	36.85	40.93	44.00	44.38	44.65	44.10	44.14
Add H_2O_2	$q_{e,r}$ (mg $g^{-1)}$	–	2.23	4.76	4.77	4.77	4.86	4.74	4.77	4.78
	RE (%)	0	20.60	43.87	44.02	43.98	44.79	43.70	44.02	44.05

Table S3
Effect of regeneration temperature (°C)

Sample	Regeneration temperature (°C)				
	25	35	45	55	65
$q_{e,r}$ (mg $g^{-1)}$	4.86	4.91	5.31	5.57	5.64
RE (%)	44.80	45.28	48.99	51.41	52.00

Table S4
Effect of pH

Sample	pH					
	2	4	6	8	10	12
$q_{e,r}$ (mg $g^{-1)}$	5.81	6.23	6.58	5.98	5.88	5.92
RE (%)	53.58	57.46	60.72	55.17	54.19	54.59

Table S5
Textural characterization of recycled 3% CQDs-TiO_2@AC

Characterization	Regeneration cycle times		
	1	2	3
BET surface area(m^2 g^{-1})	392	279	231
Micropore volume (cm^3 g^{-1})	0.1483	0.1282	0.1145

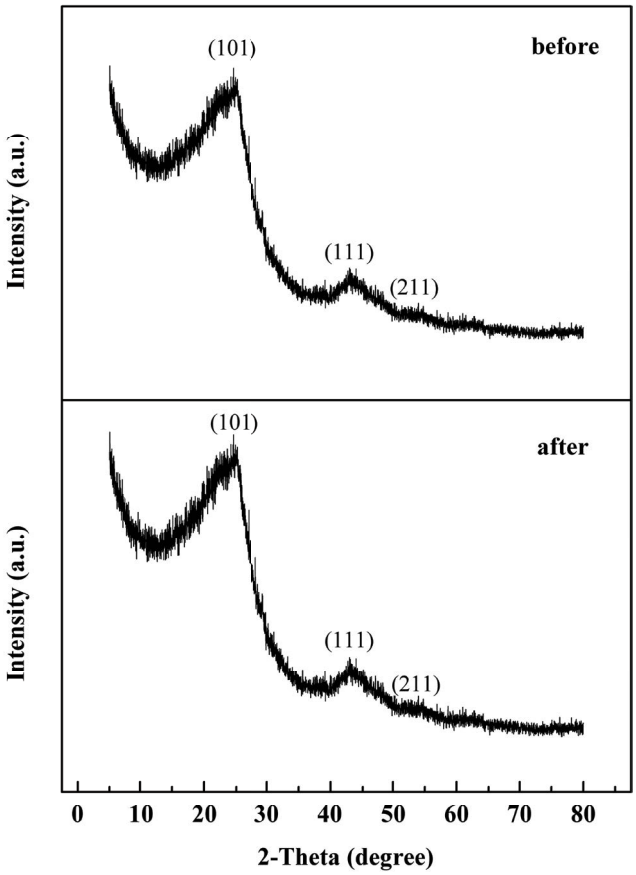

Fig. S3 XPS spectra of 3% CQDs-TiO_2@AC before and after impregnated under regeneration conditions.

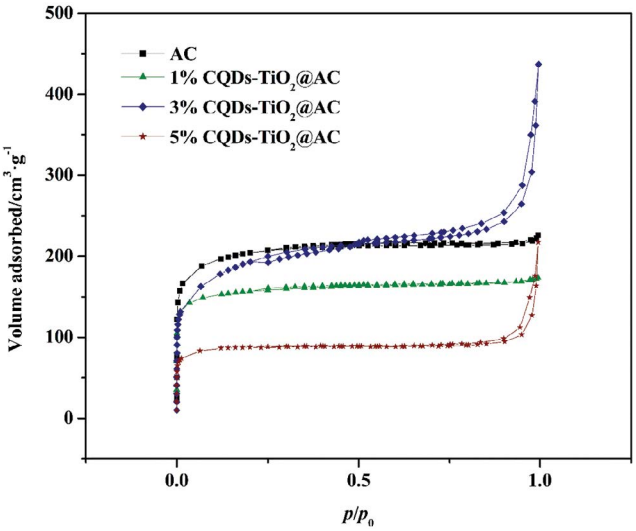

Fig. S1. Nitrogen adsorption/desorption isotherms at 77 K on samples.

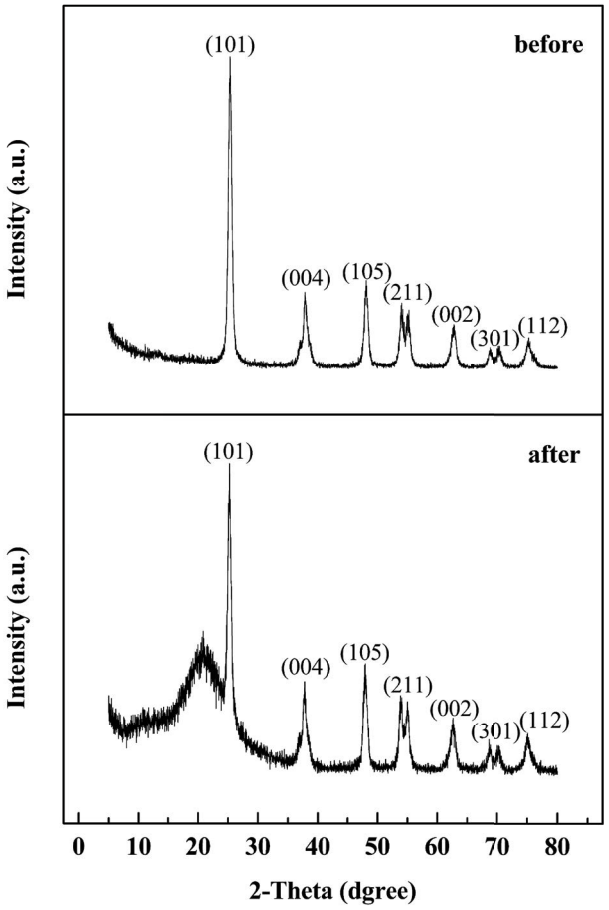

Fig. S2. XPS spectra of CQDs-TiO_2 before and after impregnated under regeneration conditions.